Review article **Open Access**

Elijah Thimsen, Bryce Sadtler and Mikhail Y. Berezin*

Shortwave-infrared (SWIR) emitters for biological imaging: a review of challenges and opportunities

DOI 10.1515/nanoph-2017-0039
Received April 2, 2017; revised May 2, 2017; accepted May 3, 2017

Abstract: Shortwave infrared radiation (SWIR) is the portion of the electromagnetic spectrum from approximately 900 nm to 2500 nm. Recent advances in imaging systems have expanded the application of SWIR emitters from traditional fields in materials science to biomedical imaging, and the new detectors in SWIR opened an opportunity of deep tissue imaging. Achieving deep photon penetration while maintaining high resolution is one of the main objectives and challenges in bioimaging used for the investigation of diverse processes in living organisms. The application of SWIR emitters in biological settings is, however, hampered by low quantum efficiency. So far, photoluminescent properties in the SWIR region have not been improved by extending concepts that have been developed for the visible (400–650 nm) and near-infrared (NIR, 700–900 nm) wavelengths, which indicates that the governing behavior is fundamentally different in the SWIR. The focus of this minireview is to examine the mechanisms behind the low efficiency of SWIR emitters as well as to highlight the progress in their design for biological applications. Several common mechanisms will be considered in this review: (a) the effect of the energy gap between the excited and ground state on the quantum efficiency, (b) the coupling of the excited electronic states in SWIR emitters to vibrational states in the surrounding matrix, and (c) the role of environment in quenching the excited states. General strategies to improve the quantum yields for a diverse type of SWIR emitters will be also presented.

***Corresponding author: Mikhail Y. Berezin,** Institute of Materials Science and Engineering; Department of Chemistry; and Mallinckrodt Institute of Radiology, Washington University School of Medicine in St. Louis, St. Louis, MO 63110, USA, e-mail: berezinm@mir.wustl.edu
Elijah Thimsen: Institute of Materials Science and Engineering; and Department of Energy, Environmental and Chemical Engineering, Washington University in St. Louis, St. Louis, MO 63130, USA
Bryce Sadtler: Institute of Materials Science and Engineering; and Department of Chemistry, Washington University in St. Louis, St. Louis, MO 63130, USA

Keywords: SWIR; Optical Window; exNIR; imaging; nanoparticles; UCNP; SWCNT; quantum dots.

1 Background

Achieving deep photon penetration is one of the main objectives in bioimaging with optical systems. Rapid deep-tissue imaging has historically been performed using ionizing radiation, typically X-rays or γ-rays. However, ionizing radiation poses a risk to biological tissue and only addresses anatomical alterations. Thus, low energy photons are preferred. The use of visible light is convenient but only feasible for superficial tissues, such as skin, due to strong absorption and scattering from tissue components.

In the last 20 years, near-infrared (NIR, 700–900 nm) fluorescent contrast agents, small molecules, and nanoparticles for *in vivo* imaging of live tissue have dominated the preclinical and clinical research landscape [1–6]. Reduced scattering by the tissue; low absorption from tissue endogenous chromophores such as water, lipids, proteins, and hemoglobin; and negligible autofluorescence has led to the selection of the NIR range as an optical window. Along with the availability of conventional silicon-based NIR enhanced CCD cameras and inexpensive light sources (i.e. 785 nm lasers), research has led to an explosion of publications, patents, and reviews from many laboratories related to NIR contrast agents [7–10] including from our group [11–13]. This explosion grew out of a well-developed understanding of the chemistry and biology of NIR fluorophores. From organic molecules to nanoparticles, early acceptance of NIR technology by the biological community has also led to the commercial development and clinical trials of many types of contrast agents. Today, more than 20 NIR contrast agents, which can be either free or conjugated to monoclonal antibodies, have been used in clinical trials, and dedicated imaging systems have emerged such as FLARE [14], NIR goggles [15], Spy Elite (Novadaq) [16], da Vinci (Intuitive Surgical) [17] for clinical diagnostics, as well as image- and robotic-guided surgeries [18, 19]. The field is well established.

Despite the progress in the NIR technology, the major drawback of shallow tissue penetration has remained the limiting factor and restricts applications to primarily small animal preclinical models (mice, small rats) [20, 21] or to assessing subcutaneous (breast, skin) [22, 23] and optically accessible tissues (i.e. esophagus, colon) [24, 25] in humans. Although not as strong in the NIR as under visible light, scattering continues to be the key obstacle in deep tissue imaging. Thus, deeper tissue penetration requires using wavelengths greater than 900 nm.

The importance of imaging in shortwave infrared radiation (SWIR) comes from the requirement to provide diagnostic tools for preclinical studies in larger animals (i.e. rabbits, dogs, and pigs, as their anatomy and physiology are more similar to human beings than rodents) [26, 27]. The importance of SWIR imaging also stems from its potential translatability to humans to replace or complement high-energy imaging modalities [such as X-ray, positron emission tomography (PET), or single-photon emission computed tomography (SPECT)].

Imaging solutions that go further into the red region than 900 nm, such as SWIR, or extended NIR (exNIR) have long been proven difficult to develop, primarily due to the lack of sensitive detectors. Commonly utilized silicon-based sensors are inefficient beyond 1100 nm, resulting in low signal [28]. Beyond 1100 nm, the Si material becomes transparent to photons as the corresponding photon energy drops below the band gap energy of this semiconducting material [29]. Operating at longer wavelengths requires coating the Si sensor with a wavelength shifting phosphor, which reduces quantum efficiency. Detectors based on germanium (Ge), indium antimonide (InSb), or mercury cadmium telluride (HgCdTe) are more sensitive but still suffer from low quantum efficiency in the SWIR range [30]. Thankfully, indium gallium arsenide (InGaAs) sensors, with their high quantum efficiency in the 900–1600 nm range, have appeared. These sensors were used mostly for military applications, such as to minimize the scattering effect of clouds or fog, a problem similar to the *in vivo* imaging challenge.

The development of InGaAs-based diode array detectors, research grade 2D cameras, and SWIR light sources (conventional quartz bulbs, temperature stabilized LEDs, laser diodes, and supercontinuum lasers [31]) sparked interest in using this technology in biology, and soon researchers recognized that in addition to the NIR, there were other optical windows in the SWIR [31–37]. Using the new detectors, several groups have demonstrated significantly higher transparency of tissue in SWIR compared to the traditional NIR range, with some of the most prominent bands of transparency at 1300 and 1550 nm [35, 37] (Figure 1). Even higher transparency may be possible at longer wavelengths (i.e. 1800 nm and 2200 nm) [36] where most of the current InGaAs detectors have low sensitivity but can rely on InSb imaging detectors for longer wavelengths.

Further steps toward the development of SWIR-based optical imaging will require more efficient contrast agents. To date, the development of biological imaging techniques utilizing absorption and emission in SWIR (SWIR→SWIR) has been limited, primarily because of the lack of efficient biocompatible emitters in this range [38]. Most of the organic SWIR dyes and many types of nanomaterials that have been developed for lasers and the telecommunication industry [39] were unsuitable for SWIR imaging due to their low (<0.1%) quantum efficiency, poor water solubility, and potential systemic toxicity. To be considered in biology, early materials, such as polymethine dyes, carbon nanotubes, quantum dots, and

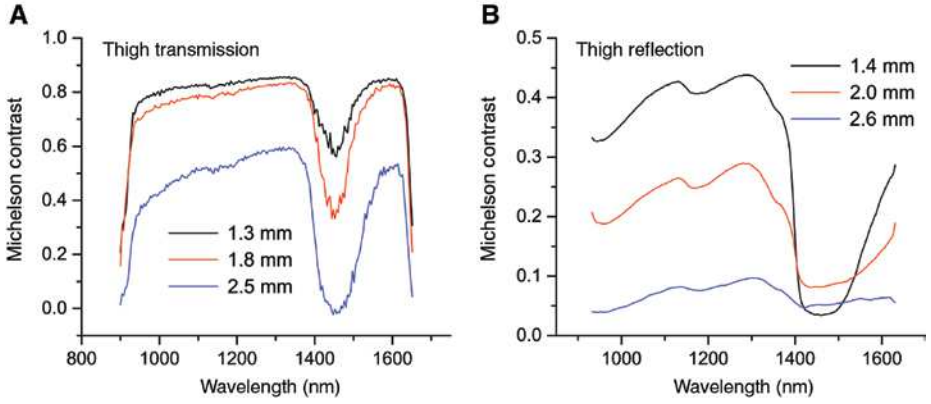

Figure 1: Transparency of biological tissue in SWIR.
The metric is based on a spatial contrast of Michelson (with permission [37]).

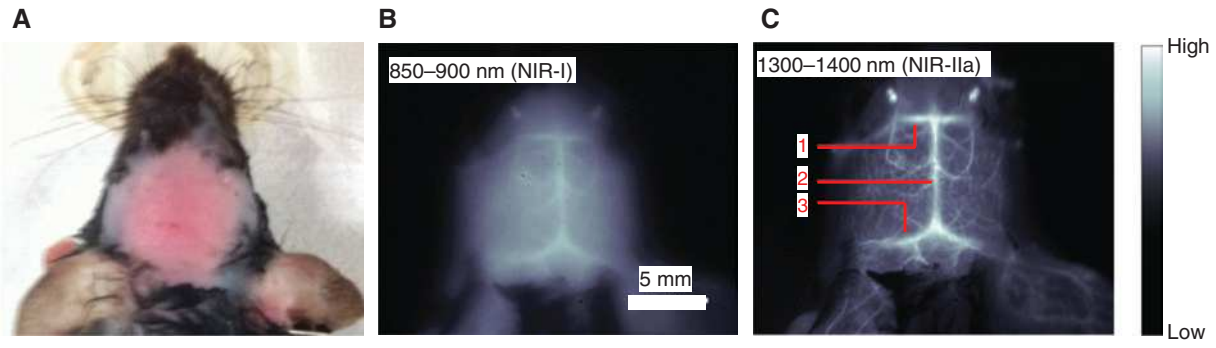

Figure 2: Imaging of deep tissue using a dual NIR-SWIR probe based on the dye IR800CW attached to single-walled carbon nanotubes (SWCNs): (A) C57Bl/6 mouse head with hair removed; (B) fluorescent images of the same mouse at 850–900 nm, (C) 1300–1400 nm. Red arrows point to specific locations in the brain that can be resolved (with permission from [40]).

upconverting nanoparticles, required some sophisticated modifications to ensure sufficient bioavailability, excretion, and low toxicity. One of the successful examples is shown in Figure 2 [40]. However, once modified, these materials demonstrated even lower quantum yield in aqueous media and poor imaging performance. The low quantum yield necessitated long light exposures, which are potentially damaging to tissue.

Over the last 10 years, the photoluminescent properties of contrast agents for biological agents in the SWIR have been substantially improved. However, they are still far below the level of visible contrast agents with 80–100% quantum efficiency. It has been realized that the governing behavior is fundamentally different in the SWIR compared to the visible region. Understanding the mechanism of low efficiency in the SWIR and demonstrating progress and potential ways to improve the signal is the focus of this minireview.

2 Mechanisms of low emission

Significant efforts have been put forth for both understanding the origins of low efficiency in current SWIR emitters and developing methods to minimize quenching effects. Out of the many pathways behind the quenching of SWIR emission, we will consider the common mechanisms that are shared by several types of contrast agents. These mechanisms include (a) the effect of the energy gap between the excited and ground states, (b) the presence of vibrational states in the surrounding matrix and their coupling with the excited electronic states, and (c) the role of environment on emitter stability and brightness. Individual specific mechanisms, such as those caused by structural defects (i.e. in SWCNs [41]), will be mentioned only briefly.

2.1 Energy gap law

The energy gap law is a fundamental constraint that states that radiationless transitions at longer wavelengths increase due to vibrational overlap between the ground and excited states [42] (Figure 3). These overlaps cause a decrease in the photoluminescent efficiency of organic and organometallic fluorophores [43] and also seem to be unavoidable in nanocrystals. This law radically restricts the number of luminescent dyes beyond 1000 nm where the overlap is almost inevitable.

Experimental verification of the energy gap law was established several decades ago, primarily for organic dye molecules emitting in the visible and NIR range. Those

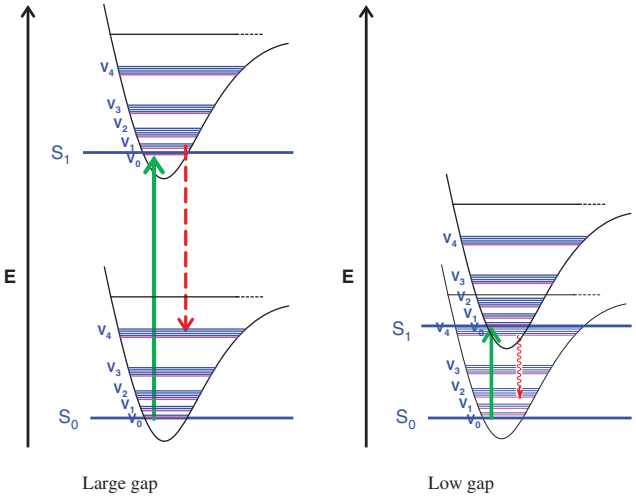

Figure 3: Illustration of the low energy gap law. Longer wavelength of emission comes with stronger overlap that weakens the emission. S_0 and S_1 are the energy levels of the ground and excited states, respectively; v_n indicates vibrationally excited levels; green arrows indicate absorption; and red arrows indicate radiative (dashed) or non-radiative relaxation (curved).

include aromatic hydrocarbons [44]; linear polyenes, including carotenoids [45]; organometallic complexes [46]; and large polymeric molecules [47]. In many of these studies, a logarithmic dependence of the non-radiative constant upon the energy gap was demonstrated. The non-radiative decay rate (k_{nr}) increases exponentially with decreasing energy separation between the excited and the ground states [48].

A critical aspect of the energy gap law is the mechanism of energy transfer from the excited state. It has been agreed in general that the excited state serves as a donor that provides energy to the vibrational modes of the acceptors within the same molecule or nearby solvent molecules. However, questions about the nature of the acceptors remain largely under discussion. In fact, there is an unsettled debate over whether the critical "accepting" modes (the vibrational modes into which the majority of the excited-state energy is disposed) is C-H or C-C stretching in character. Are there solvent molecules involved? For organic molecules, the experimental results demonstrate that C-C stretching modes play a major, if not the dominant, role in the process [49].

2.2 The nature of vibrational modes in tissue

The excitation energy of the SWIR emitter might be transferred radiatively or non-radiatively to the tissue components. In the radiative process, the emitted photons are reabsorbed by the tissue through the overlap between the emission band of the emitter and the absorption bands of the tissue components. The efficiency of this process depends upon the wavelength of emission and thickness of the tissue. In the non-radiative pathway, the energy dissipation occurs via Förster resonance energy transfer (FRET) without emitting a photon. Because of the short, nanometer-range nature of this effect, the process is primarily governed by the nearest layer of ligands or tissue molecules through their absorption bands.

Absorption bands seen in SWIR in biological tissue components such as water, lipids, proteins, etc. (Figure 4) are the overtones and combination bands of their corresponding fundamental vibrations (tones). The overtone and combination bands are considerably blue-shifted with respect to the tones. The latter are typically observed at mid-infrared (400–4000 cm^{-1} or 2500–25,000 nm) by IR or Raman spectroscopy. Overtone and combination bands are due to the anharmonicity of the vibration that is the deviation from an ideal harmonic oscillator, such as seen in a bond with two identical atoms. The anharmonicity increases when the bond connects atoms with dramatically different masses, such as in the case of X-H

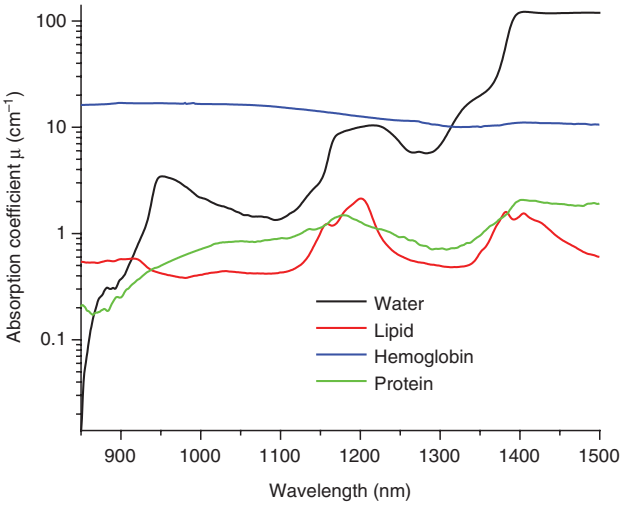

Figure 4: Absorption spectra of major endogenous tissue chromophores: water, hemoglobin, protein (represented here by albumin), and lipids (with permission from [35]).

bonds where X is C, O, or N. Because of the anharmonicity of tissue components, the SWIR range is dominated by signals from bonds involving hydrogen atoms such as O-H (water, carbohydrates), C-H (lipids), and N-H (proteins).

The radiative energy transfer or photon reabsorption cannot be avoided, as the emitter in the deep tissue is surrounded by a large number of tissue molecules. The non-radiative process, however, can be efficiently controlled as was first proposed and demonstrated by Guyot-Sionnest et al. [50] and later confirmed by Aharoni et al. [51]. In their seminal paper, Guyot-Sionnest et al. have demonstrated that the direct near-field energy transfer of the electronic excitation to vibrational absorption by ligand or matrix is a predictable quantifiable effect; it is fast and applies to any transition [50]. For example, the non-radiative recombination of excitons, defined as bound electron-hole pairs, in quantum dots results from coupling to C-H vibrations in the surface-bound ligands, which have characteristic frequencies in the wavelength region of interest. Placing an inorganic spacer transparent to SWIR photons or modifying the surface ligands is an example of promising strategies to minimize the probability of non-radiative de-excitation (*vide infra*).

2.3 Role of vibrational modes in quenching of SWIR emitters

The mechanisms by which photoexcitations are coupled to vibrational modes are graphically summarized by Figure 5. The accepted opinion is that a resonant energy transfer mechanism, akin to Förster energy transfer, is the process by

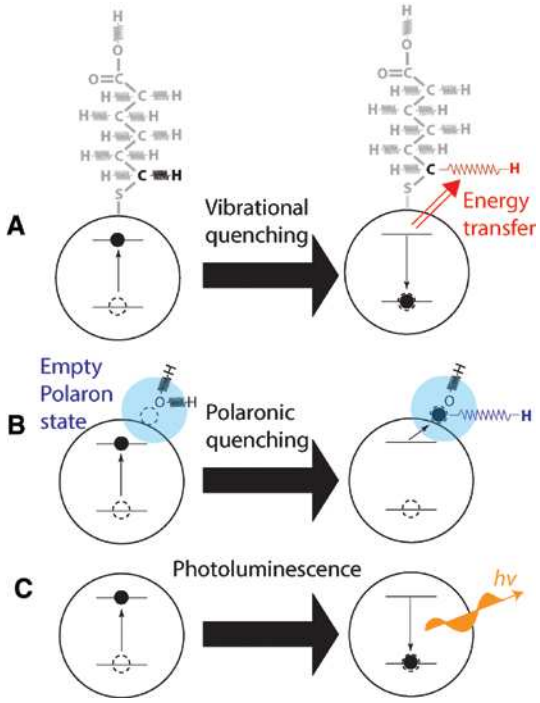

Figure 5: Exciton relaxation pathways in quantum dots photoluminescent in the SWIR.
(A) Resonant energy transfer. (B) Polaronic quenching.
(C) Photoemission.

which the exciton couples to ligand vibrations (Figure 5A) [50–53]. For quantum dots, it has been proposed that the energy transfer proceeds via polaron states formed by strong coupling of vibrational modes to surface trap states (Figure 5B) [54]. In our opinion, coupling of photoexcitations to vibrational states is one of the primary causes of low quantum yield. This hypothesis is consistent with the experimental observations of a number of researchers [50–57]. For example, InAs nanocrystals with peak emission at 1200 nm showed significantly higher efficiency in halogenated solvent compared to toluene [51]. In the range of the C-H vibrations (1150–1200 nm), the photoluminescence lifetime was approximately three times longer in the halogenated solvent compared to toluene, indicating that excitons were coupled more strongly to C-H stretch modes [51]. In another example, when HgTe nanocrystals emitting at 1060 nm were transferred from H_2O to D_2O, the quantum yield increased from 5% to 20% [54].

2.4 Other mechanisms affecting quantum efficiency

Solvent molecules might stabilize or destabilize the excited states of SWIR emitters. For example, polymethine dye molecules are known to have high sensitivity to solvent polarity, which significantly affects quantum efficiency [58, 59]. Considering that the SWIR absorption bands in polymethine dyes arise from electronic transition involving the π electrons along the polymethine chain, the cations in the ground state of the polymethine dyes resonate between two limiting canonical structures. Based on NMR and crystallography studies of NIR dyes, the ground state of the cyanines are predominantly in all-trans configurations [60, 61]. In the excited state, the bond order lowers and reduces the electron density in the double bonds along the polymethine chain, making the molecule more sensitive to the surrounding molecules and ions.

The change in bond order facilitates vibrational rotations and allows the molecule to twist during its lifetime in the excited state. The twisted conformation is likely to undergo trans-cis isomerization, leading to non-radiative decay. A polar medium facilitates *trans-cis* transformation, effectively decreasing the quantum efficiency, while a non-polar environment stabilizes the excited state, thereby increasing the quantum yield as well as fluorescence lifetime and photostability. Formation of a microenvironment (polymeric or silica) around the emitter is a known strategy to increase the quantum efficiency of polymethine dyes and has been explored in many NIR contrast agents [62, 63].

2.5 Strategies to decrease quenching

Reabsorption of photons by the tissue absorbers cannot be eliminated or even minimized and is entirely dependent on the tissue thickness. In contrast, non-radiative quenching can be effectively controlled through the architecture of the ligands surrounding the emitter. The partial contribution from each of the pathways is difficult to evaluate, but based on published work, we believe that non-radiative emission dominates the quenching process. Thus, eliminating non-radiative quenching might significantly increase quantum efficiency of the contrast agent.

A set of rules to minimize the effect of quenching of the emitter from the media or ligands was originally established by Hasegawa et al. for SWIR emitting lanthanides [64] but can also be expanded to other classes of SWIR emitters. The rules suggest to (i) avoid hydrogen-rich solvent molecules in the first coordination sphere; (ii) eliminate O-H groups around the emitting core, as these groups are the most efficient quenchers; and (iii) minimize the presence of C-H groups. Although the effects of C-H oscillators are smaller than those of O-H, C-H bonds are abundant in the biological media. Some of the successful examples

of using these strategies are based on replacing hydrogen atoms with deuterium or fluorine.

Deuteration or fluorination of ligands coordinating SWIR emitters has been demonstrated in a number of studies, primarily in lanthanides. As deuterium is twice as heavy as hydrogen, such substitution (from C-H to C-D, and O-H to O-D) decreases the strength of the oscillator. This decrease leads to a decline in absorbance band intensities from the vibrational state and diminishes the influence of the overtones on emission. Hence, deuteration of ligands has been demonstrated to increase the quantum yield in a number of SWIR emitting complexes, including Er^{3+}, Nd^{3+}, and Yt^{3+} emitters [65, 66]. Fluorine is even larger than deuterium, so the effect is stronger and is considered to be more efficient than deuteration [67]. Complete fluorination might be quite complex and require substantial synthetic efforts; instead, partial fluorination can be used. This partial fluorination of ligands has led to a significant improvement of the quantum efficiency of Er^{3+} complexes emitting at 1535 nm [68, 69].

Encapsulation of the emitter within an inorganic matrix transparent to SWIR photons follows the same idea. The matrix shields the emission core by increasing the distance between the donor and the acceptor. Given that energy transfer is inversely proportional to the distance as $1/r^6$, several nanometers of the layer might be sufficient. Consistent with this idea, PbS quantum dots protected with As_2S_3 shells showed a significant increase in the quantum efficiency [70].

3 Emitters in SWIR

Today, there are several classes of SWIR emitting dyes and nanomaterials that have been or can potentially be used in SWIR imaging (Figure 6). Reported compounds include cyanine dyes [74], lanthanide complexes [75], Pt complexes [73], certain types of quantum dots [76], small gold nanoparticles [77], and single-walled carbon nanotubes (SWCNTs) [32, 33]. We will briefly describe some of these most common contrast agents while focusing on strategies to improve quantum efficiency.

3.1 Organic dyes

Historically, organic dyes were the first small molecules developed in early 1980s to emit in the SWIR range, primarily as the media for tunable dye-based lasers [78, 79]. Organic dyes that are fluorescent in the SWIR, such as IR-26, IR-1048 or IR-1061, are stable but highly hydrophobic and suffer from extremely low quantum yield – less than 0.05% [52, 80]. In addition to a significant overlap

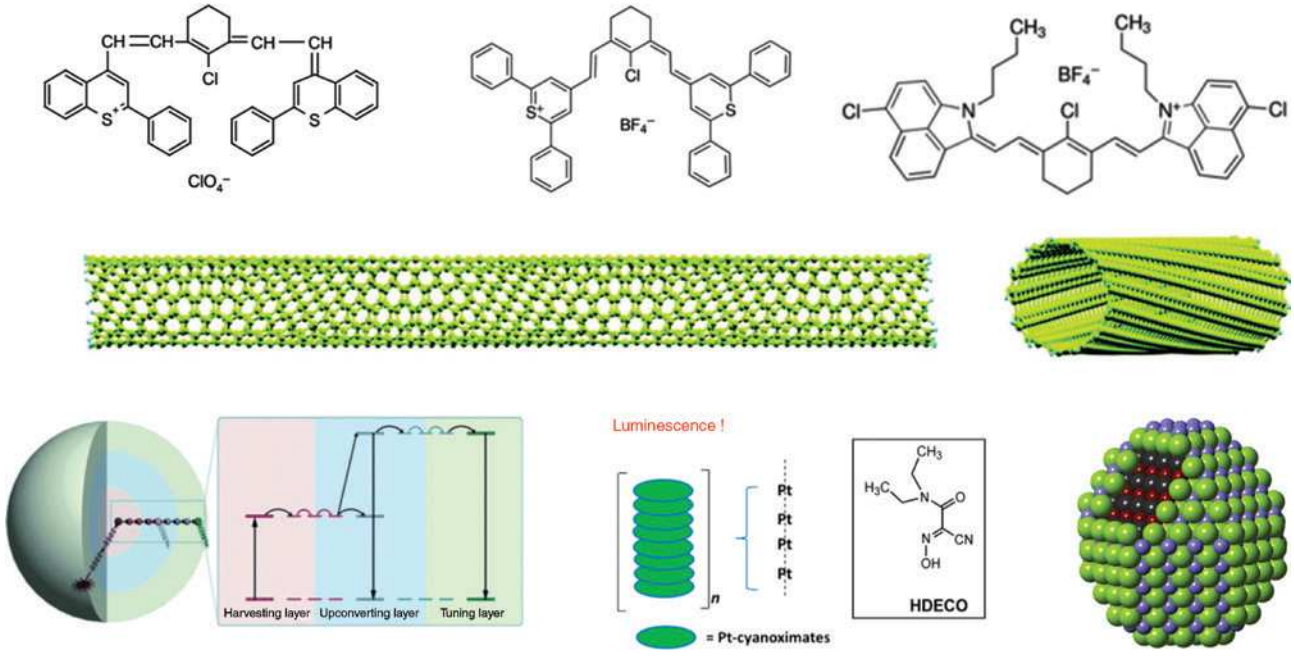

Figure 6: SWIR emitters: commercially available SWIR dyes emitting at >1000 nm IR-26, IR-1048, IR-1061.
Schematics of single-walled carbon nanotubes (with permission from [71]), upconverting nanoparticles (with permission from [72]), nanowire formed by self-assembly of a Pt complex (with permission from [73]), and quantum dots.

between the excited and ground states (low energy gap) and quenching by vibrational states of solvent molecules, the emission of these dyes is strongly influenced by solvent polarity.

Encapsulation of the hydrophobic SWIR dye IR-1061 into a water-soluble polymer nanoparticle with a hydrophobic cavity has led to a relatively high quantum yield, enabling real-time imaging of hind-limb hemodynamics [81]. A recent development in using organic dyes was achieved with a new SWIR dye, CH1055, conjugated to PEG for facilitated bioavailability and excretion [82].

3.2 Single-walled carbon nanotubes

SWCNTs are SWIR-emitting materials that have been extensively investigated for sensing in biological media *in vitro* [83, 84] and *in vivo* [32, 85]. Due to their sharp multiple SWIR spectral features across a broad bandwidth from 800 to 1600 nm, SWCNTs also showed the potential for *in vivo* hyperspectral imaging [86, 87]. However, photon-conversion efficiency of SWCNTs is relatively low (<0.1%) [88], which makes SWCNTs suboptimal for demanding bioimaging applications.

Theoretical and experimental studies suggest that carbon nanotube photoluminescence is inefficient because of low-lying dark excitons that enhance non-radiative transmission [71, 89]. Various structural defects that develop during their synthesis or processing can accumulate over the relatively long length (100–1000 nm) of the nanotubes [41, 90]. Studying the decay rate of the fluorescence from individual SWCNTs, Wang et al. suggested that the low fluorescence quantum yield is controlled by quenching from the structural defects [41]. The structural defects can also react with oxygen to form a hydroperoxide carbocation in a process known as hole doping [91], which further decreases the quantum yield. Nanotube aggregation has also been reported as a cause of quenching [92].

Several strategies have been published to improve the quantum efficiency of nanotubes. Minimizing the oxidative defects by hole passivation with reducing agents [93] and oxygen-excluding surfactants [94] has improved the quantum yield. Purification of the nanotubes through gradient centrifugation and minimizing the aggregation has also been fruitful for increasing the efficiency to 20% [94]. Another breakthrough came from covalent functionalization of SWCNTs with a controlled number of aryl functional groups that produced a new and bright photoluminescence peak through introduction of a bright defect state [95].

3.3 Lanthanide nanoparticles

Lanthanide-based nanomaterials have [96] emerged relatively recently for optical imaging due to their high stability and low toxicity [97]. The most common lanthanide-based nanoparticles are based on the photon upconversion effect, in which at least two incident photons of relatively low energy are absorbed and converted into one emitted photon with higher energy [98]. Typical upconverting nanoparticles (UCNPs) are oxides or fluorides, i.e. $NaYF_4$ doped with lanthanides, such as Yb^{3+} ions that work as sensitizers and co-doped with Er^{3+} or Tm^{3+} ions that serve as emitters (activators). In the most common designs of UCNP $NaYF_4$:Yb/Er, Tm, the excitation occurs at ca. 980 nm due to the absorption by Yb^{3+}. The long-lived metastable energy state of the excited Yb-ions allows additional photons to be absorbed. The absorbed multiphoton energy is then transferred from the sensitizer to the activator, resulting in emission at shorter wavelengths. For example, Tm^{3+} emits at 474 nm and 798 nm [96] while Er^{3+} emits at 410, 520, 540, and 660 nm [96].

Ideally, deep tissue imaging requires excitation and emission in SWIR (SWIR→SWIR). In reality, this is difficult to achieve with the currently developed UCNPs. The excitation of most UCPNs occurs in SWIR (980 nm), but their emission lies in the Vis or NIR range (SWIR→Vis, NIR). Similarly structured nanoparticles, such as lanthanide-based downconverting nanoparticles (DCNPs), absorb in the visible range and emit in the SWIR (Vis →SWIR). For example, LaF_3 nanoparticles doped with Nd^{3+}, Ho^{3+}, or Er^{3+} emit at 1330, 1450, and 1525 nm correspondingly but require an excitation with a 513-nm laser to achieve good signal [99, 100].

Addressing this challenge, photon downconversion has been accomplished using a NIR laser (802 nm) to achieve NIR→SWIR [101]. Recently Kamimuro et al. used PEGylated Y_2O_3:Yb, Er nanoparticles to show a strong signal at 1550 nm *in vivo* upon irradiation with a 980-nm laser, thus realizing SWIR→SWIR imaging [102]. Furthermore, Naczynski et al. developed a library of rare earth nanoreporters with tunable, discrete SWIR emission over the broad range of 1000–2300 nm.

The luminescence efficiency of UCNPs and DCNPs emitting in SWIR is generally low. Several strategies have been devised to improve the quantum efficiency. To suppress the vibrational quenching caused by the O-H groups from water on the surfaces of NdF_3 nanoparticles, they were coated with silica [103]. This treatment led to a 1.6 times higher intensity than that of bare NdF_3. In a similar strategy, Chen et al. grew a thin layer of $NaGdF_4$ shells on top of $NaGdF_4$:Nd^{3+} of nanocrystals to prepare

highly efficient DCNPs with an absolute quantum yield of 40% [104].

3.4 Quantum dots

Synthetic protocols for known materials that have band gaps appropriate for emission in the SWIR were established a relatively long time ago [105, 106]. Today, there are quantum dots composed of different types of semiconductors including InAs and InP, PbSe and PbS, HgTe, Ag_2S and Ag_2Se, $CuInS_2$, and $CuInSe_2$. Photoluminescent semiconductor nanocrystals are in general much brighter than other SWIR emitters such as dyes, SWCNTs and DCNPs, in which their brightness, in part, stems from high molar absorptivities. In the context of bioimaging applications, the quantum yield values that have been demonstrated to date are still rather low – less than 10% at a peak wavelength of 1550 nm when measured in an inert, air-free environment.

A major problem in using SWIR quantum dots in a biological setting is their notorious instability in aqueous media. Virtually all known quantum dots materials degrade in the presence of water and air [107, 108]. For example, PbS and PbSe quantum dots are prone to oxidation and other reactions (i.e. etching, photobleaching) resulting in the loss of emission [109, 110]. Thus, the principal challenge is to develop a robust shell that protects the emitting core. While for the visible emitting quantum dots composed of CdSe, the growth of a passivating shell such as CdS/ZnS has been well established, with the quantum yield reaching unity [111], this approach has been proven to be more difficult for SWIR emitters. There are only a handful reports that have been able to show the application of SWIR quantum dots in bioimaging [112].

Robust inorganic shells to chemically isolate the core emitter from the biological environment present a promising approach. Benayas et al. used two layers of protection to develop bright water-dispersible core/shell1/shell2 PbS/CdS/ZnS quantum dots [113]. Similarly, using multiple layers of protection, Aharoni et al. prepared InAs/CdSe/ZnSe nanoemitters [114].

Oxide coatings on quantum dots are known to exhibit excellent chemical stability that can be applied to protect the core [115]. A key challenge with metal oxide coatings is to ensure they are free from OH groups, which are expected to exacerbate vibrational PL quenching. Addressing this challenge, Yin et al. developed a high-precision method of coating quantum dots using an atomic layer deposition technique to improve the photoluminescence stability [116]. Although the method has been demonstrated on visible quantum dots, it could potentially be expanded to SWIR emitters as well.

4 Concluding remarks

The last decade saw the emergence of SWIR emitting small molecules and nanoparticles that have great potential in the field of bioimaging. A great number of synthetic procedures have been developed; however, for most of the compounds, the quantum efficiency remains low. Hence, significant effort has been spent to develop and deploy biocompatible small molecules and nanomaterials that are bright in the SWIR. Protection of the emitters from aggressive biological media and/or minimizing energy transfer from the emitter to tissue chromophores in order to retain high quantum efficiency presents a significant challenge. Other critical barriers that limit biological applications include (i) relatively low reproducibility and scalability; (ii) poor long-term stability in aqueous media, buffers, and biological media; (iii) difficulty in attaching targeting groups; (iv) potential immunogenicity; and (v) limited clinical translation that requires no toxic metals in the formulation regardless of the product stability.

Given that the synthesis of bright emitters, especially nanoparticles, involves a complex compositional space, computational approaches, such as those based on machine learning and data mining, may be of great value in the search for new material systems. In the field of emitters, such an approach has the potential to quickly predict the brightest stable and non-toxic nanoparticles with the desired properties as a function of size, composition, and heterostructure. Accurate modeling of the photophysics and photochemistry of SWIR nanoemitters will facilitate and accelerate the synthetic procedures to identify high-performance, nontoxic materials.

Overall, the progress in the development of SWIR emitters has been dramatic and exciting. Further progress in this field will require innovative strategies to not only enhance the radiative-transition rate of SWIR-emitting species but also make them highly biocompatible.

Acknowledgments: We thank NCI/NIH CA198419 (MB), NSF Research Infrastructure Improvement Award #IIA-1355406 (MB), for the financial support in writing this review. We also thank William Buhro (Washington University) for the discussion and Sharon Bloch for editing the manuscript.

References

[1] Solomon M, Liu Y, Berezin MY, Achilefu S. Optical imaging in cancer research: basic principles, tumor detection, and therapeutic monitoring. Med Princ Pract 2011;20:397–415.

[2] Sevick-Muraca EM, Houston JP, Gurfinkel M. Fluorescence-enhanced, near infrared diagnostic imaging with contrast agents. Curr Opin Chem Biol 2002;6:642–50.

[3] Achilefu S, Dorshow RB, Bugaj JE, Rajagopalan R. Novel receptor-targeted fluorescent contrast agents for in vivo tumor imaging. Invest Radiol 2000;35:479–85.

[4] Gustafson TP, Dergunov SA, Akers WJ, et al. Blood triggered rapid release porous nanocapsules. RSC Adv 2013;3:5547–55.

[5] Luo S, Zhang E, Su Y, Cheng T, Shi C. A review of NIR dyes in cancer targeting and imaging. Biomaterials 2011;32:7127–38.

[6] Berezin MY. (ed.) Nanotechnology for biomedical imaging and diagnostics: from nanoparticle design to clinical applications. Hoboken, New Jersey, Wiley, 2015, 520.

[7] Lu D, He L, Zhang G, et al. Aptamer-assembled nanomaterials for fluorescent sensing and imaging. Nanophotonics 2017;6:109–21.

[8] Kim S, Lim YT, Soltesz EG, et al. Near-infrared fluorescent type II quantum dots for sentinel lymph node mapping. Nat Biotech 2004;22:93–7.

[9] Solomon M, Guo K, Sudlow GP, et al. Detection of enzyme activity in orthotopic murine breast cancer by fluorescence lifetime imaging using a fluorescence resonance energy transfer-based molecular probe. J Biomed Opt 2011;16:066019-1-6.

[10] Weissleder R, Tung CH, Mahmood U, Bogdanov A. In vivo imaging of tumors with protease-activated near-infrared fluorescent probes. Nat Biotech 1999;17:375–8.

[11] Zhegalova NG, He S, Zhou H, Kim DM, Berezin MY. Minimization of self-quenching fluorescence on dyes conjugated to biomolecules with multiple labeling sites via asymmetrically charged NIR fluorophores. Contrast Media Mol Imaging 2014;9:355–62.

[12] Zhegalova NG, Gonzales G, Berezin MY. Synthesis of nitric oxide probes with fluorescence lifetime sensitivity. Org Biomol Chem 2013;11:8228–34.

[13] Zhou H, Gunsten SP, Zhegalova NG, et al. Visualization of pulmonary clearance mechanisms via noninvasive optical imaging validated by near-infrared flow cytometry. Cytometry A 2015;87:419–27.

[14] Troyan SL, Kianzad V, Gibbs-Strauss SL, et al. The FLARE™ intraoperative near-infrared fluorescence imaging system: a first-in-human clinical trial in breast cancer sentinel lymph node mapping. Ann Surg Oncol 2009;16:2943–52.

[15] Liu Y, Bauer AQ, Akers WJ, et al. Hands-free, wireless goggles for near-infrared fluorescence and real-time image-guided surgery. Surgery 2011;149:689–98.

[16] Gurtner GC, Jones GE, Neligan PC, et al. Intraoperative laser angiography using the SPY system: review of the literature and recommendations for use. Ann Surg Innov Res 2013;7:1.

[17] Rossi EC, Ivanova A, Boggess JF. Robotically assisted fluorescence-guided lymph node mapping with ICG for gynecologic malignancies: a feasibility study. Gynecol Oncol 2012;124:78–82.

[18] Gioux S, Choi HS, Frangioni JV. Image-guided surgery using invisible near-infrared light: fundamentals of clinical translation. Mol Imaging 2010;9:237–55.

[19] Autorino R, Zargar H, White WM, et al. Current applications of near-infrared fluorescence imaging in robotic urologic surgery: a systematic review and critical analysis of the literature. Urology 2014;84:751–9.

[20] Zhou H, Yan Y, Ee X, et al. Imaging of radicals following injury or acute stress in peripheral nerves with activatable fluorescent probes. Free Radical Biol Med 2016;101:85–92.

[21] Magalotti S, Gustafson TP, Cao Q, et al. Evaluation of inflammatory response to acute ischemia using near-infrared fluorescent reactive oxygen sensors. Mol Imaging Biol 2013;15:423–30.

[22] Robinson JT, Hong G, Liang Y, Zhang B, Yaghi OK, Dai H. In vivo fluorescence imaging in the second near-infrared window with long circulating carbon nanotubes capable of ultrahigh tumor uptake. J Am Chem Soc 2012;134:10664–9.

[23] Lamberts LE, Koch M, de Jong JS, et al. Tumor-specific uptake of fluorescent bevacizumab-IRDye800CW microdosing in patients with primary breast cancer: a phase I feasibility study. Clin Cancer Res 2017;23:2730–41.

[24] Habibollahi P, Figueiredo JL, Heidari P, et al. Optical imaging with a cathepsin B activated probe for the enhanced detection of esophageal adenocarcinoma by dual channel fluorescent upper GI endoscopy. Theranostics 2012;2:227–34.

[25] Iftimia N, Iyer AK, Hammer DX, et al. Fluorescence-guided optical coherence tomography imaging for colon cancer screening: a preliminary mouse study. Biomed Opt Express 2012;3:178–91.

[26] Kobayashi E, Hishikawa S, Teratani T, Lefor AT. The pig as a model for translational research: overview of porcine animal models at Jichi Medical University. Transplant Res 2012;1:8.

[27] Conn PM. (ed.) Animal models for the study of human disease. Elsevier, London, Waltham, MA, 2013, xviii, 1089.

[28] Bai Y, Bernd SG, Hosack JR, Farris MC, Montroy JT, Bajaj J. Hybrid CMOS focal plane array with extended UV and NIR response for space applications. Proc SPIE 2004;5167:83–93.

[29] Luryi S, Kastalsky A, Bean JC. New infrared detector on a silicon chip. IEEE Trans Electron Dev 1984;31:1135–9.

[30] Hansen MP, Malchow DS. Overview of SWIR detectors, cameras, and applications. Proc SPIE 2008;6939:693901-1-11.

[31] Sordillo LA, Lindwasser L, Budansky Y, Leproux P, Alfano RR. Near-infrared supercontinuum laser beam source in the second and third near-infrared optical windows used to image more deeply through thick tissue as compared with images from a lamp source. J Biomed Opt 2015;20:030501-1-3.

[32] Welsher K, Sherlock SP, Dai HJ. Deep-tissue anatomical imaging of mice using carbon nanotube fluorophores in the second near-infrared window. Proc Natl Acad Sci USA 2011;108:8943–8.

[33] Smith AM, Mancini MC, Nie S. Bioimaging: second window for in vivo imaging. Nat Nanotechnol 2009;4:710–1.

[34] Shi L, Alfano RRE. (eds.) Deep imaging in tissue and biomedical materials: using linear and nonlinear optical methods. 1st ed. Singapore, Pan Stanford Publishing Pte., 2017.

[35] Cao Q, Zhegalova NG, Wang ST, Akers WJ, Berezin MY. Multispectral imaging in the extended near-infrared window based on endogenous chromophores. J Biomed Opt 2013;18:101318-1-7.

[36] Shi L, Sordillo LA, Rodriguez-Contreras A, Alfano R. Transmission in near-infrared optical windows for deep brain imaging. J Biophotonics 2016;9:38–43.

[37] Zhang H, Salo D, Kim DM, Komarov S, Tai YC, Berezin MY. Penetration depth of photons in biological tissues from hyperspectral imaging in shortwave infrared in transmission and reflection geometries. J Biomed Opt 2016;21:126006.
[38] Naczynski DJ, Tan MC, Zevon M, et al. Rare-earth-doped biological composites as in vivo shortwave infrared reporters. Nat Commun 2013;4:2199:1-10.
[39] Jackson SD. The spectroscopic and energy transfer characteristics of the rare earth ions used for silicate glass fibre lasers operating in the shortwave infrared. Laser Photonics Rev 2009;3:466–82.
[40] Hong G, Diao S, Chang J, et al. Through-skull fluorescence imaging of the brain in a new near-infrared window. Nat Photon 2014;8:723–30.
[41] Wang F, Dukovic G, Brus LE, Heinz TF. Time-resolved fluorescence of carbon nanotubes and its implication for radiative lifetimes. Phys Rev Lett 2004;92:177401:1-4.
[42] Bixon M, Jortner J. Intramolecular radiationless transitions. J Chem Phys 1968;48:715–26.
[43] Lakowicz JR. Principles of fluorescence spectroscopy. 3rd ed. New York, Springer, 2006, xxvi, 954.
[44] Siebrand W, Williams D. Radiationless transitions in polyatomic molecules. III. Anharmonicity, isotope effects, and singlet-to-ground-state transitions in aromatic hydrocarbons. J Chem Phys 1968;49:1860–71.
[45] Dinur U, Scharf B. Radiationless transitions in linear polyenes. J Chem Phys 1983;79:2600–8.
[46] Cummings SD, Eisenberg R. Tuning the excited-state properties of platinum(II) diimine dithiolate complexes. J Am Chem Soc 1996;118:1949–60.
[47] Englman R, Jortner J. The energy gap law for radiationless transitions in large molecules. Mol Phys 1970;18:145–64.
[48] Frank HA, Chynwat V, Desamero RZB, Farhoosh R, Erickson J, Bautista J. On the photophysics and photochemical properties of carotenoids and their role as light-harvesting pigments in photosynthesis. Pure Appl Chem 1997;69:2117–24.
[49] Kober EM, Caspar JV, Lumpkin RS, Meyer TJ. Application of the energy gap law to excited-state decay of osmium (II)-polypyridine complexes: calculation of relative nonradiative decay rates from emission spectral profiles. J Phys Chem 1986;90:3722–34.
[50] Guyot-Sionnest P, Wehrenberg B, Yu D. Intraband relaxation in CdSe nanocrystals and the strong influence of the surface ligands. J Chem Phys 2005;123:074709:1–7.
[51] Aharoni A, Oron D, Banin U, Rabani E, Jortner J. Long-range electronic-to-vibrational energy transfer from nanocrystals to their surrounding matrix environment. Phys Rev Lett 2008;100:057404:1–4.
[52] Semonin OE, Johnson JC, Luther JM, Midgett AG, Nozik AJ, Beard MC. Absolute photoluminescence quantum yields of IR-26 Dye, PbS, and PbSe quantum dots. J Phys Chem Lett 2010;1:2445–50.
[53] Lhuillier E, Keuleyan S, Liu H, Guyot-Sionnest P. Mid-IR colloidal nanocrystals. Chem Mater 2013;25:1272–82.
[54] Wen Q, Kershaw SV, Kalytchuk S, et al. Impact of D2O/H2O solvent exchange on the emission of HgTe and CdTe quantum dots: polaron and energy transfer effects. ACS Nano 2016;10:4301–11.
[55] Jeong KS, Guyot-Sionnest P. Mid-infrared photoluminescence of CdS and CdSe colloidal quantum dots. ACS Nano 2016;10:2225–31.
[56] Deng Z, Guyot-Sionnest P. Intraband luminescence from HgSe/CdS core/shell quantum dots. ACS Nano 2016;10:2121–7.
[57] Shen G, Guyot-Sionnest P. HgS and HgS/CdS colloidal quantum dots with infrared intraband transitions and emergence of a surface plasmon. J Phys Chem C 2016;120:11744–53.
[58] Berezin MY, Lee H, Akers W, Achilefu S. Near infrared dyes as lifetime solvatochromic probes for micropolarity measurements of biological systems. Biophys J 2007;93:2892–9.
[59] Lee H, Berezin MY, Henary M, Strekowski L, Achilefu S. Fluorescence lifetime properties of near-infrared cyanine dyes in relation to their structures. J Photochem Photobiol A 2008;200:438–44.
[60] Kim SH, Han SK, Kim JJ, Lim WT, Heo NH, Koh KN. Crystal structure of a photoconductive dithiosquarylium dye: 2,4-bis(1,3,3-trimethyl-2-indolinylidenemethyl)cyclobutenediylium-1,3-dithiolate. Dyes Pigm 1998;39:259–66.
[61] Benniston AC, Harriman A, Gulliya KS. Photophysical properties of merocyanine 540 derivatives. J Chem Soc Faraday Trans 1994;90:953–61.
[62] Palantavida S, Tang R, Sudlow GP, Akers WJ, Achilefu S, Sokolov I. Ultrabright NIR fluorescent mesoporous silica nanoparticles. J Mater Chem B 2014;2:3107–14.
[63] Yu J, Zhang X, Hao X, et al. Near-infrared fluorescence imaging using organic dye nanoparticles. Biomaterials 2014;35:3356–64.
[64] Hasegawa Y, Wada Y, Yanagida S. Strategies for the design of luminescent lanthanide (III) complexes and their photonic applications. J Photochem Photobiol C 2004;5:183–202.
[65] Tan RHC, Motevalli M, Abrahams I, Wyatt PB, Gillin WP. Quenching of IR luminescence of erbium, neodymium, and ytterbium β-diketonate complexes by ligand C–H and C–D bonds. J Phys Chem B 2006;110:24476–9.
[66] Hu JY, Ning Y, Meng YS, et al. Highly near-IR-emissive Ytterbium (III) complexes with unprecendented quantum yields. Chem Sci 2017;8:2702–9.
[67] Hernandes I, Gillin W. Organic chromophores-based sensitization of NIR-emitting lanthanides: toward highly efficient halogenated environments. In: Bunzli J-C, Pecharsky V, eds. Handbook on the physics and chemistry of rare earths. Amsterdam, The Netherlands, Elsevier, 2015.
[68] Mancino G, Ferguson AJ, Beeby A, Long NJ, Jones TS. Dramatic increases in the lifetime of the Er3+ ion in a molecular complex using a perfluorinated imidodiphosphinate sensitizing ligand. J Am Chem Soc 2005;127:524–5.
[69] Peng Y, Hu J, Lu H, et al. Functionalisation of ligands through click chemistry: long-lived NIR emission from organic Er (III) complexes with a perfluorinated core and a hydrogen-containing shell. RSC Adv 2017;7:128–31.
[70] Kovalenko MV, Schaller RD, Jarzab D, Loi MA, Talapin DV. Inorganically functionalized PbS–CdS colloidal nanocrystals: integration into amorphous chalcogenide glass and luminescent properties. J Am Chem Soc 2012;134:2457–60.
[71] Scholes GD, Tretiak S, McDonald TJ, et al. Low-lying exciton states determine the photophysics of semiconducting single wall carbon nanotubes. J Phys Chem C 2007;111:11139–49.
[72] Wen H, Zhu H, Chen X, et al. Upconverting near-infrared light through energy management in core–shell–shell nanoparticles. Angew Chem Int Ed 2013;52:13419–23.
[73] Klaus DR, Keene M, Silchenko S, Berezin M, Gerasimchuk N. 1D polymeric platinum cyanoximate: a strategy toward lumines-

cence in the near-infrared region beyond 1000 nm. Inorg Chem 2015;54:1890–900.
[74] Casalboni M, De Matteis F, Prosposito P, Quatela A, Sarcinelli F. Fluorescence efficiency of four infrared polymethine dyes. Chem Phys Lett 2003;373:372–8.
[75] Bischof C, Wahsner J, Scholten J, Trosien S, Seitz M. Quantification of C–H quenching in near-IR luminescent ytterbium and neodymium cryptates. J Am Chem Soc 2010;132:14334–5.
[76] Jiang P, Zhu CN, Zhang ZL, Tian ZQ, Pang DW. Water-soluble Ag2S quantum dots for near-infrared fluorescence imaging in vivo. Biomaterials 2012;33:5130–5.
[77] Wang G, Huang T, Murray RW, Menard L, Nuzzo RG. Near-IR luminescence of monolayer-protected metal clusters. J Am Chem Soc 2004;127:812–3.
[78] Kranitzky W, Kopainsky B, Kaiser W, Drexhage K, Reynolds G. A new infrared laser dye of superior photostability tunable to 1.24 μm with picosecond excitation. Opt Commun 1981;36:149–52.
[79] Schäfer FP. New developments in laser dyes. Laser Chem 1983;3:265–78.
[80] Hatami S, Wurth C, Kaiser M, et al. Absolute photoluminescence quantum yields of IR26 and IR-emissive Cd1-xHgxTe and PbS quantum dots – method- and material-inherent challenges. Nanoscale 2015;7:133–43.
[81] Tao Z, Hong G, Shinji C, et al. Biological imaging using nanoparticles of small organic molecules with fluorescence emission at wavelengths longer than 1000 nm. Angew Chem Int Ed Engl 2013;52:13002–6.
[82] Antaris AL, Chen H, Cheng K, et al. A small-molecule dye for NIR-II imaging. Nat Mater 2016;15:235–42.
[83] Satishkumar BC, Brown LO, Gao Y, Wang CC, Wang HL, Doorn SK. Reversible fluorescence quenching in carbon nanotubes for biomolecular sensing. Nat Nano 2007;2:560–4.
[84] Brege JJ, Gallaway C, Barron AR. Fluorescence quenching of single-walled carbon nanotubes with transition-metal ions. J Phys Chem C 2009;113:4270–6.
[85] Robinson JT, Welsher K, Tabakman SM, et al. High performance in vivo near-IR (>1 μm) imaging and photothermal cancer therapy with carbon nanotubes. Nano Res 2010;3:779–93.
[86] Bachilo SM, Strano MS, Kittrell C, Hauge RH, Smalley RE, Weisman RB. Structure-assigned optical spectra of single-walled carbon nanotubes. Science 2002;298:2361–6.
[87] Roxbury D, Jena PV, Williams RM, et al. Hyperspectral microscopy of near-infrared fluorescence enables 17-chirality carbon nanotube imaging. Sci Rep 2014;5:14167-1-6.
[88] Welsher K, Liu Z, Sherlock SP, et al. A route to brightly fluorescent carbon nanotubes for near-infrared imaging in mice. Nat Nanotechnol 2009;4:773–80.
[89] Perebeinos V, Tersoff J, Avouris P. Radiative lifetime of excitons in carbon nanotubes. Nano Lett 2005;5:2495–9.
[90] Cognet L, Tsyboulski DA, Rocha JDR, Doyle CD, Tour JM, Weisman RB. Stepwise quenching of exciton fluorescence in carbon nanotubes by single-molecule reactions. Science 2007;316:1465–8.
[91] Dukovic G, White BE, Zhou Z, et al. Reversible surface oxidation and efficient luminescence quenching in semiconductor single-wall carbon nanotubes. J Am Chem Soc 2004;126:15269–76.
[92] Crochet J, Clemens M, Hertel T. Quantum yield heterogeneities of aqueous single-wall carbon nanotube suspensions. J Am Chem Soc 2007;129:8058–9.
[93] Lee AJ, Wang X, Carlson LJ, et al. Bright fluorescence from individual single-walled carbon nanotubes. Nano Lett 2011;11:1636–40.
[94] Ju SY, Kopcha WP, Papadimitrakopoulos F. Brightly fluorescent single-walled carbon nanotubes via an oxygen-excluding surfactant organization. Science 2009;323:1319–23.
[95] Piao Y, Meany B, Powell LR, et al. Brightening of carbon nanotube photoluminescence through the incorporation of sp3 defects. Nat Chem 2013;5:840–5.
[96] Song Z, Anissimov YG, Zhao J, et al. Background free imaging of upconversion nanoparticle distribution in human skin. J Biomed Opt 2013;18:061215-1-10.
[97] Zhou B, Shi B, Jin D, Liu X. Controlling upconversion nanocrystals for emerging applications. Nat Nano 2015;10:924–36.
[98] Haase M, Schäfer H. Upconverting nanoparticles. Angew Chem Int Ed Engl 2011;50:5808–29.
[99] Stouwdam JW, van Veggel FCJM. Near-infrared emission of redispersible Er3+, Nd3+, and Ho3+ doped LaF3 nanoparticles. Nano Lett 2002;2:733–7.
[100] Wang R, Zhang F. Lanthanide-based near infrared nanomaterials for bioimaging. In: Zhang F., ed. Near-infrared nanomaterials: preparation, bioimaging and therapy applications. Cambridge, UK, The Royal Society of Chemistry, 2016, 1–39.
[101] Wang F, Zhang Y, Fan X, Wang M. Facile synthesis of water-soluble LaF3:Ln3+ nanocrystals. J Mater Chem 2006;16:1031–4.
[102] Kamimura M, Kanayama N, Tokuzen K, Soga K, Nagasaki Y. Near-infrared (1550 nm) in vivo bioimaging based on rare-earth doped ceramic nanophosphors modified with PEG-b-poly(4-vinylbenzylphosphonate). Nanoscale 2011;3:3705–13.
[103] Yu XF, Chen LD, Li M, et al. Highly efficient fluorescence of NdF3/SiO2 core/shell nanoparticles and the applications for in vivo NIR detection. Adv Mater 2008;20:4118–23.
[104] Chen G, Ohulchanskyy TY, Liu S, et al. Core/Shell NaGdF4:Nd3+/NaGdF4 nanocrystals with efficient near-infrared to near-infrared downconversion photoluminescence for bioimaging applications. ACS Nano 2012;6:2969–77.
[105] Pichaandi J, van Veggel FCJM. Near-infrared emitting quantum dots: recent progress on their synthesis and characterization. Coordin Chem Rev 2014;263–264:138–50.
[106] Rogach AL, Eychmüller A, Hickey SG, Kershaw SV. Infrared-emitting colloidal nanocrystals: synthesis, assembly, spectroscopy, and applications. Small 2007;3:536–57.
[107] Bae WK, Joo J, Padilha LA, et al. Highly effective surface passivation of PbSe quantum dots through reaction with molecular chlorine. J Am Chem Soc 2012;134:20160–8.
[108] Leschkies KS, Kang MS, Aydil ES, Norris DJ. Influence of atmospheric gases on the electrical properties of PbSe quantum-dot films. J Phys Chem C 2010;114:9988–96.
[109] Stouwdam JW, Shan J, van Veggel FCJM, Pattantyus-Abraham AG, Young JF, Raudsepp M. Photostability of colloidal PbSe and PbSe/PbS core/shell nanocrystals in solution and in the solid state. J Phys Chem C 2007;111:1086–92.
[110] Aydt AP, Blair S, Zhang H, Chernomordik BD, Beard MC, Berezin MY. Synthesis and spectroscopic evaluation of PbS quantum dots emitting at 1300 nm for optimized imaging in optical window II. Proc SPIE 2016:9723–97230Z-10.

[111] Greytak AB, Allen PM, Liu W, et al. Alternating layer addition approach to CdSe/CdS core/shell quantum dots with near-unity quantum yield and high on-time fractions. Chem Sci 2012;3:2028–34.
[112] Hong G, Robinson JT, Zhang Y, et al. In vivo fluorescence imaging with Ag2S quantum dots in the second near-infrared region. Angew Chem Int Ed Engl 2012;51:9818–21.
[113] Benayas A, Ren F, Carrasco E, et al. PbS/CdS/ZnS quantum dots: a multifunctional platform for in vivo near-infrared low-dose fluorescence imaging. Adv Funct Mater 2015;25:6650–9.
[114] Aharoni A, Mokari T, Popov I, Banin U. Synthesis of InAs/CdSe/ZnSe Core/Shell1/Shell2 structures with bright and stable near-infrared fluorescence. J Am Chem Soc 2006;128:257–64.
[115] Akkerman QA, Genovese A, George C, et al. From binary Cu2S to ternary Cu–In–S and quaternary Cu–In–Zn–S nanocrystals with tunable composition via partial cation exchange. ACS Nano 2015;9:521–31.
[116] Yin B, Sadtler B, Berezin MY, Thimsen E. Quantum dots protected from oxidative attack using alumina shells synthesized by atomic layer deposition. Chem Commun 2016;52:11127–30.